

The depletion of star-forming gas by AGN activity in radio sources

S. J. Curran*

School of Chemical and Physical Sciences, Victoria University of Wellington, PO Box 600, Wellington 6140, New Zealand

Abstract

Cold, neutral interstellar gas, the reservoir for star formation, is traced through the absorption of the 21-centimetre continuum radiation by neutral hydrogen (HI). Although detected in one hundred cases in the host galaxies of distant radio sources, only recently have column densities approaching the maximum value observed in Lyman- α absorption systems ($N_{\text{HI}} \sim 10^{22} \text{ cm}^{-2}$) been found. Here we explore the implications these have for the hypothesis that the detection rate of HI absorption is dominated by photo-ionisation from the active galactic nucleus (AGN). We find, with the addition all of the current searches for HI absorption at $z \geq 0.1$, a strong correlation between the HI absorption strength and the ionising photon rate, with the maximum value at which HI is detected remaining close to the theoretical value in which all of the neutral gas would be ionised in a large spiral galaxy ($Q_{\text{HI}} = 2.9 \times 10^{56}$ ionising photons s^{-1}). We also rule out other effects (excitation by the radio continuum and changing gas properties) as the dominant cause for the decrease in the detection rate with redshift. Furthermore, from the maximum theoretical column density we find that the five high column density systems have spin temperatures close to those of the Milky Way ($T_{\text{spin}} \lesssim 300 \text{ K}$), whereas, from our model of a gaseous galactic disk, the HI detection at $Q_{\text{HI}} = 2.9 \times 10^{56} \text{ s}^{-1}$ yields $T_{\text{spin}} \sim 10\,000 \text{ K}$, consistent with the gas being highly ionised.

Keywords: galaxies: active – quasars: absorption lines – radio lines: galaxies – ultraviolet: galaxies – galaxies: fundamental parameters – galaxies: ISM

1 INTRODUCTION

Since the first high redshift ($z \gtrsim 3$) survey for cold neutral (star-forming) gas, via the absorption of the 21-centimetre transition of neutral hydrogen in the host galaxies of distant radio sources, it has been posited that the dearth of detections is due to the selection of ultra-violet (UV) luminous sources. In these objects, the UV radiation from the AGN is sufficient to ionise the gas to below the detection limits of large radio telescopes (Curran et al., 2008b). While a steady decrease with redshift, and hence UV luminosity, may be expected, an abrupt cut-off in the detection of HI above $L_{\text{UV}} \sim 10^{23} \text{ W Hz}^{-1}$ (ionising photon rates of $Q_{\text{HI}} \gtrsim 10^{56} \text{ s}^{-1}$) is apparent. Curran & Whiting (2012) showed that such a critical luminosity would arise from an exponential gas distribution, with the observed value being close that required to ionise all of the gas in the Milky Way, i.e. a large spiral.

Since then, this observational result has been confirmed, not only over specific “homogeneous” subsets of sources (compact, extended, flat spectrum, etc., Curran et al. 2013b, 2016; Aditya et al. 2016; Aditya & Kanekar 2018a; Grasha et al. 2019; Murthy et al. 2021, 2022), but also unbiased samples, limited only by flux (Curran et al., 2011, 2013a, 2017a,b, 2019; Allison et al., 2012; Geréb et al., 2015). The complete ionisation of the gas within the host galaxies of

these objects would prevent star formation within them and is strongly indicative of a selection effect, where the traditional need for a reliable optical redshift, to which to tune the radio-band receiver, causes a bias towards the most UV luminous sources (Curran et al., 2008b). This suggests a population of undetected gas-rich galaxies in the distant Universe, too faint to be detected via optical spectroscopy.

There is, however, still some debate over this interpretation: Curran et al. (2008b) also noted that all of the sources above the critical UV luminosity were type-1 objects (quasars), suggesting that the gas could be undetected due to the obscuring circum-nuclear torus, invoked by unified schemes of AGN (Osterbrock, 1978; Antonucci & Miller, 1985; Miller & Goodrich, 1987), not intercepting our sight-line to the AGN. However, below the critical UV luminosity the detection rate was similar to that in type-2 objects (galaxies), suggesting that the bulk of the absorption occurs in the large-scale galactic disc, which is randomly orientated to the pc-scale torus (Curran & Whiting, 2010). Furthermore, rather than photo-ionisation from the AGN being the dominant cause of the decrease in detection rate with redshift, Aditya & Kanekar (2018a,b); Aditya et al. (2024) propose excitation of the hydrogen by 1.4 GHz photons (Purcell & Field, 1956; Field, 1959) or some other (unspecified) evolutionary effect. While the former has been ruled out (Curran et al. 2008b, 2019,

*Stephen.Curran@vuw.ac.nz

see also Sect. 3.1.3), the latter effects would have to apply across the whole sample, irrespective of source classification in order to usurp the ionisation hypothesis.

Most recently, there have been five detections of HI absorption (Chowdhury et al., 2020; Murthy et al., 2021; Su et al., 2022; Aditya et al., 2024), where the column density would exceed the theoretical limit of $N_{\text{HI}} \sim 10^{22} \text{ cm}^{-2}$ (Schaye, 2001), for moderate spin temperatures. In this paper we reassess the ionisation hypothesis in light of these and the vastly increased sample of published HI searches.

2 ANALYSIS

2.1 The data

Adding the recent searches, comprising 441 objects (Chowdhury et al., 2020; Murthy et al., 2021, 2022; Mahony et al., 2022; Su et al., 2022; Aditya et al., 2024; Deka et al., 2024), to those compiled in Curran et al. (2019) there are now 924 $z \geq 0.1$ sources in the literature which have been searched for associated HI 21-cm absorption. These are made up of 100 detections and 824 non-detections.

2.2 Photometry and fitting

To obtain the ionising photon rate for each of the 924 sources, their photometry were scraped from the *NASA/IPAC Extragalactic Database* (NED), the *Wide-Field Infrared Survey Explorer* (WISE, Wright et al. 2010) *Two Micron All Sky Survey* (2MASS, Skrutskie et al. 2006) and the *Galaxy Evolution Explorer* (GALEX, data release GR6/7)¹ databases. After shifting the data back into the source’s rest-frame, each flux density measurement, S_ν , was then converted to a specific luminosity, via $L_\nu = 4\pi D_L^2 S_\nu / (z + 1)$, where D_L is the luminosity distance to the source (see Fig. 1).² To obtain the ionising photon rate we use (Osterbrock, 1989),

$$Q_{\text{HI}} \equiv \int_{\nu_{\text{ion}}}^{\infty} \frac{L_\nu}{h\nu} d\nu, \quad (1)$$

where ν is the frequency (with $\nu_{\text{ion}} = 3.29 \times 10^{15} \text{ Hz}$ for HI) and h the Planck constant. Fitting the rest-frame UV data with a power-law fit, $L_\nu \propto \nu^\alpha$, gives

$$\log_{10} L_\nu = \alpha \log_{10} \nu + C, \quad (2)$$

where C is the log-space intercept and α the gradient (the spectral index). Integrating this over ν_{ion} to ∞ gives the ionising photon rate as

$$Q_{\text{HI}} = \frac{-10^C}{\alpha h} \nu_{\text{ion}}^\alpha, \quad (3)$$

shown by the shaded region in Fig. 1. In order to ensure a sufficient sample size, while not contaminating the UV with

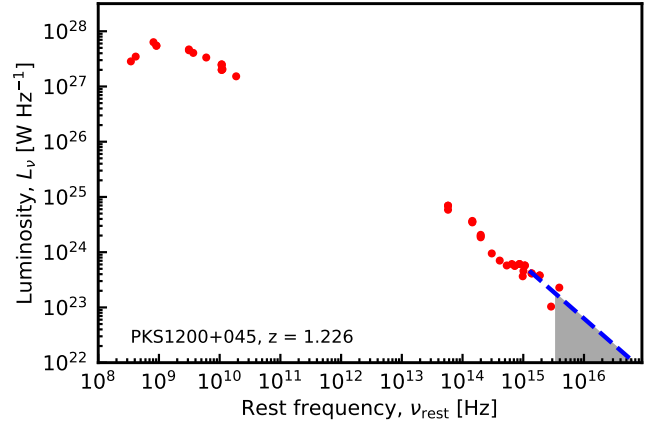


Figure 1. Example of the rest-frame photometry. The dotted line shows the power-law fit to the UV data and the shaded region $\nu \geq 3.29 \times 10^{15} \text{ Hz}$ over which the ionising photon rate is calculated. Here we show PKS 1200+045, which with $Q_{\text{HI}} = 2.9 \times 10^{56} \text{ s}^{-1}$ is the highest ionising photon rate at which HI absorption has been detected (see Sect. 3.3).

optical-band data, we fit all photometry with $\log_{10} \nu \geq 15.1$ (shown by the dotted line in the figure), which left 180 sources with sufficient UV data. Of these, 19 have been detected in HI.

2.3 HI absorption strength

The strength of the HI 21-cm absorption is given by the profile’s velocity integrated optical depth ($\int \tau dv$), which is analogous to the equivalent width in optical-band spectroscopy. This is related to the total neutral hydrogen column density via

$$N_{\text{HI}} = 1.823 \times 10^{18} T_{\text{spin}} \int \tau dv, \quad (4)$$

where the spin temperature, T_{spin} , quantifies the excitation from the lower hyperfine level of the hydrogen atom (Purcell & Field, 1956).

We do not measure the intrinsic optical depth directly, but rather the observed optical depth, τ_{obs} , which is the ratio of the line depth, ΔS , to the observed background flux, S_{obs} . The two are related via

$$\tau \equiv -\ln \left(1 - \frac{\tau_{\text{obs}}}{f} \right) = -\ln \left(1 - \frac{\Delta S}{f S_{\text{obs}}} \right), \quad (5)$$

where the covering factor, f , is the fraction of S_{obs} intercepted by the absorber. In the optically thin regime, where $\tau_{\text{obs}} \lesssim 0.3$, $\tau \approx \tau_{\text{obs}}/f$, so that Equ. 4 can be approximated as

$$N_{\text{HI}} \approx 1.823 \times 10^{18} \frac{T_{\text{spin}}}{f} \int \tau_{\text{obs}} dv. \quad (6)$$

For the non-detections, the upper limit to the line strength is obtained via $\tau_{\text{obs}} = 3\sigma_{\text{rms}}/S_{\text{obs}}$, where σ_{rms} is the rms noise level of the spectrum. In order to place each of the limits on an equal footing each is re-sampled to the same spectral resolution ($\Delta v = 20 \text{ km s}^{-1}$), which is then used as

¹<http://galex.stsci.edu/GR6/#mission>

²We use $H_0 = 67.4 \text{ km s}^{-1} \text{ Mpc}^{-1}$ and $\Omega_m = 0.3125$ (Planck Collaboration et al., 2020) throughout the paper.

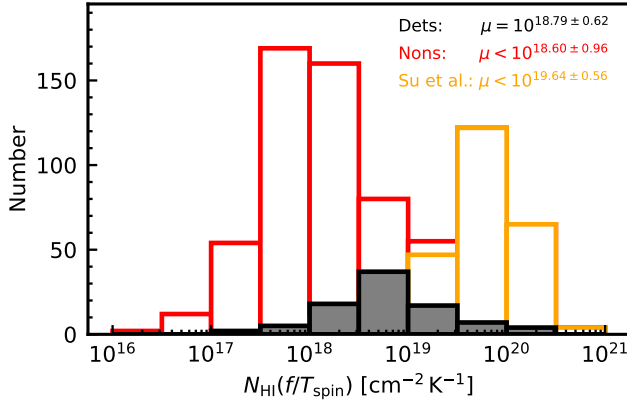


Figure 2. The distributions of the normalised line strengths for the detections (filled histogram) and the upper limits (unfilled), which have been separated into the upper limits of Su et al. (2022) and the rest of the sample. The legend shows the mean ($\pm 1\sigma$) value of each distribution.

the FWHM to obtain the integrated optical depth limit per channel (see Curran 2012).

Common practice is to convert the observed velocity integrated optical depth to a column density, by assuming the spin temperature (and, presumably, $f = 1$, e.g. Su et al. 2023). However, since we have no information on this, or the covering factor³, we define the *normalised line strength*

$$1.823 \times 10^{18} \int \tau_{\text{obs}} dv, \text{ which gives } N_{\text{HI}} \left(\frac{f}{T_{\text{spin}}} \right). \quad (7)$$

Showing the distributions in Fig. 2, we see that while, in general, the non-detections have been searched sufficiently deeply to detect HI absorption, the sample of Su et al. (2022) may not have been.⁴ In order to reduce any bias by including weaker limits, in the rest of the analysis we only consider non-detections searched to $N_{\text{HI}} \leq 10^{19} (T_{\text{spin}}/f) \text{ cm}^{-2}$.

3 RESULTS AND DISCUSSION

3.1 Factors affecting the detection of HI

3.1.1 Source classification

In Fig. 3 we show the derived ionising photon rates versus the look-back time/redshift. At low redshifts, we can see the high detection rate reported previously (e.g. Vermeulen et al. 2003; Maccagni et al. 2017). At best, we would expect a $\approx 50\%$ rate from the random orientation of the absorbing medium, whether this be in the obscuring torus or the large-scale galactic disk. However, it is clear that there is a sharp decrease in

³Where N_{HI} is available, either from 21-cm emission at $z \lesssim 0.1$ or Lyman- α absorption (at $z \gtrsim 1.7$ with ground-based instruments), T_{spin}/f can be measured, although this varies greatly between objects: 40 – 300 K within the Milky Way (Strasser & Taylor, 2004) and $10 \lesssim T_{\text{spin}}/f \lesssim 10^4$ K at high redshift (Curran, 2019), as well across individual objects: In near-by galaxies this is $T_{\text{spin}}/f \approx 2000$ K within the stellar disk at galactocentric radii of $r \lesssim 10$ kpc before peaking at $T_{\text{spin}}/f \approx 7000$ K at $r \approx 15$ kpc (Curran, 2020), where the OB stars are concentrated (Morgan et al., 1953).

⁴Most likely due to their selection of very faint continuum sources ($S_{\text{obs}} \gtrsim 10$ mJy).

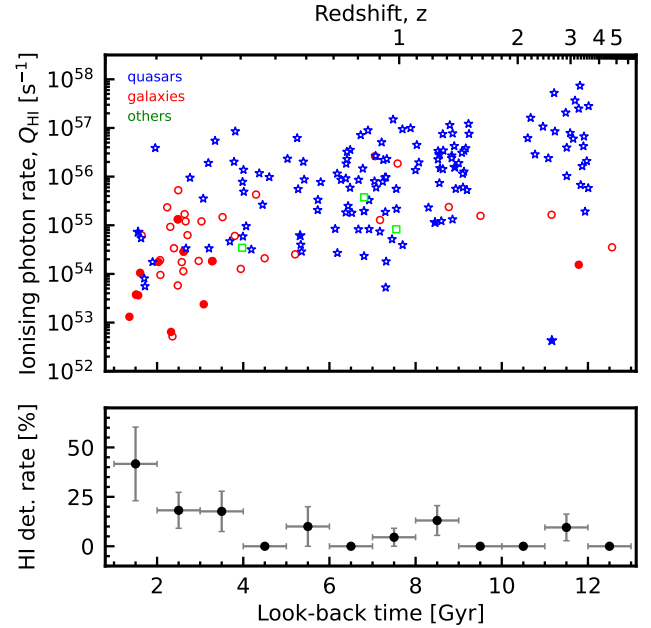


Figure 3. The ionising photon rate versus the look-back time. The filled symbols show the HI detections and the unfilled the non-detections, with the shapes designating the source classification: quasars – stars, galaxies – circles, other – squares. The lower panel shows the HI detection rate at various look-back times, where the error bars on the ordinate show the Poisson standard errors and abscissa the range over which these apply.

the detection rate with redshift, which may be caused by the preferential selection of type-1 objects (quasars), where the AGN is not obscured by the torus.

The galaxy and quasar detection rates are shown in Fig. 4. Ignoring the 50 and 100% values, which comprise only one or two objects, we see that both detection rates drop with increasing Q_{HI} . This is much steeper for galaxies, although these start from much higher values. Below the critical UV luminosity, Curran et al. (2008b) found a $53 \pm 10\%$ detection rate for galaxies and $33 \pm 13\%$ for quasars at $L_{\text{UV}} \lesssim 10^{23} \text{ W Hz}^{-1}$. The current numbers are smaller as we use the more stringent $\log_{10} \nu \geq 15.1$, cf. $\log_{10} \nu \geq 14.8$, for the UV data, as well as the ionising photon rate (by integrating the UV photometry), rather than the monochromatic luminosity, which requires more complete UV photometry. If we ignore the small number statistics⁵, this suggests that the orientation of the torus may play a role, but given that quasars are nevertheless detected in HI absorption, this cannot be the whole story. Note also that Murthy et al. (2022) do not detect absorption in any of their 29 targets, considered to be galaxies and therefore expected to yield several detections. However, the choice of targeting extended objects may bias towards lowering covering factors, the effect of which is suspected of reducing the observed optical depth in extended radio sources (Curran et al., 2013c).

⁵The first three quasar bins have a total of just 4 quasars for $Q_{\text{HI}} < 10^{54} \text{ s}^{-1}$, 21 for $10^{54} < Q_{\text{HI}} < 10^{56} \text{ s}^{-1}$ and 40 for $10^{55} < Q_{\text{HI}} < 10^{55} \text{ s}^{-1}$.

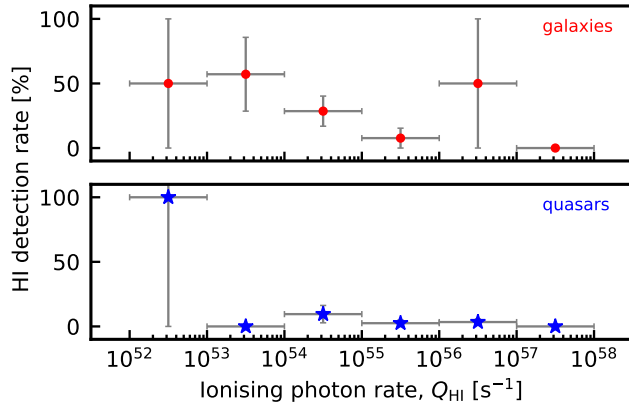


Figure 4. The detection rate versus the ionising photon rate for the galaxies and the quasars. The error bars are as described in Fig. 3. For the galaxies the exact 50% detection rates are due to a single detection and non-detection in the range and the 100% detection rate for the quasars is due to only having a single object in the range. The HI detected galaxy in the $Q_{\text{HI}} = 10^{56} - 10^{57} \text{ s}^{-1}$ bin is PKS 1200+045 (see Sect. 3.3).

Lastly, there is the simple explanation that quasars are generally more luminous than galaxies (e.g. Antonucci 1993) and, by scaling, have correspondingly higher ionisation rates. This is apparent in Fig. 5, where the UV and radio luminosities are strongly correlated [$p(\tau) = 2.17 \times 10^{-14}$]. That is, the Malmquist bias towards brighter objects at high redshift, and fainter objects at low redshift, means that the brighter quasars will be more UV luminous resulting in a lower HI detection rate.

3.1.2 Ionising photon rate

In Fig. 6, we show the distribution of the normalised line strengths versus the ionising photon rates for the sources which have sufficient UV photometry. For the 19 detections alone, a Kendall-tau test gives a probability of $p(\tau) = 0.046$ for the $N_{\text{HI}}/(fT_{\text{spin}}) - Q_{\text{HI}}$ anti-correlation occurring by chance. This is significant at 1.99σ , assuming Gaussian statistics. If we include the upper limits, as censored data points, via the *Astronomy SURVival Analysis* (ASURV) package (Isobe et al., 1986), the probability becomes $p(\tau) = 3.66 \times 10^{-6}$ (4.63σ).

Of the five absorbers with $N_{\text{HI}} \gtrsim 10^{20} (T_{\text{spin}}/f) \text{ cm}^{-2}$, only one has sufficient UV photometry to obtain the ionising photon rate (WISEA J145239.38+062738.2). With $Q_{\text{HI}} = 2.4 \times 10^{53} \text{ s}^{-1}$, this is well below the $Q_{\text{HI}} \sim 10^{56} \text{ s}^{-1}$ cut off. However, from the binning in Fig. 6, the anti-correlation between absorption strength and ionising photon rate is clear.⁶ Lastly, below the maximum detected value of $Q_{\text{HI}} = 2.9 \times 10^{56} \text{ s}^{-1}$ there are 19 detections and 124 non-detections, giving a detection rate of 13.3%. Above the maximum detected value, there are 40 non-detections and, of course, 0 detections. For $p = 0.133$, the binomial probability of obtaining 0 detections out of 40 at $Q_{\text{HI}} > 2.9 \times 10^{56} \text{ s}^{-1}$ is 3.32×10^{-3} (2.94σ).

⁶The limits are included via the Kaplan & Meier (1958) estimator.

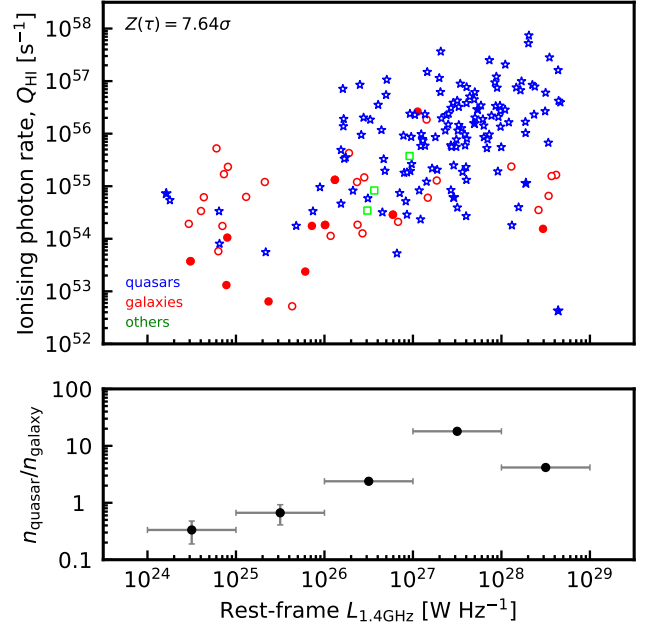


Figure 5. The ionising photon rate versus the 21-cm continuum luminosity. The bottom panel shows the ratio of quasars to galaxies in each $L_{1.4 \text{ GHz}}$ bin.

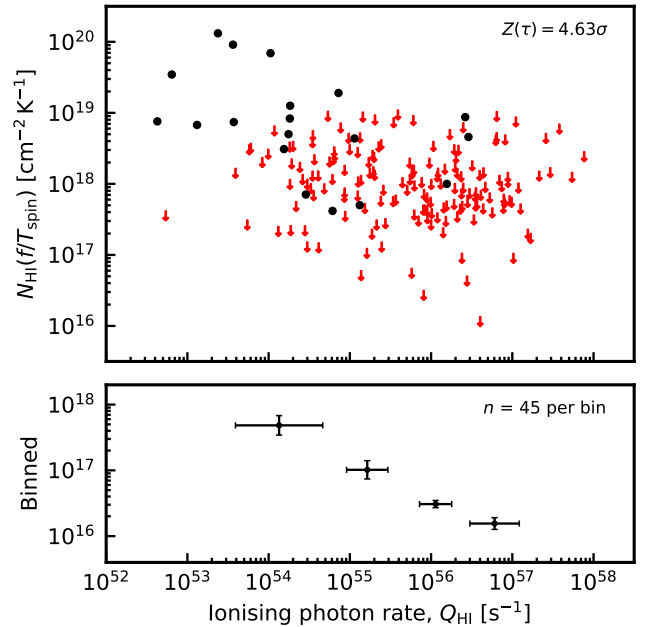


Figure 6. The normalised absorption strength versus the ionising photon rate. The circles show the detections and the arrows the 3σ upper limits re-sampled to $\Delta v = 20 \text{ km s}^{-1}$. The lower panel shows the data in equally sized bins with $\pm 1\sigma$ error bars.

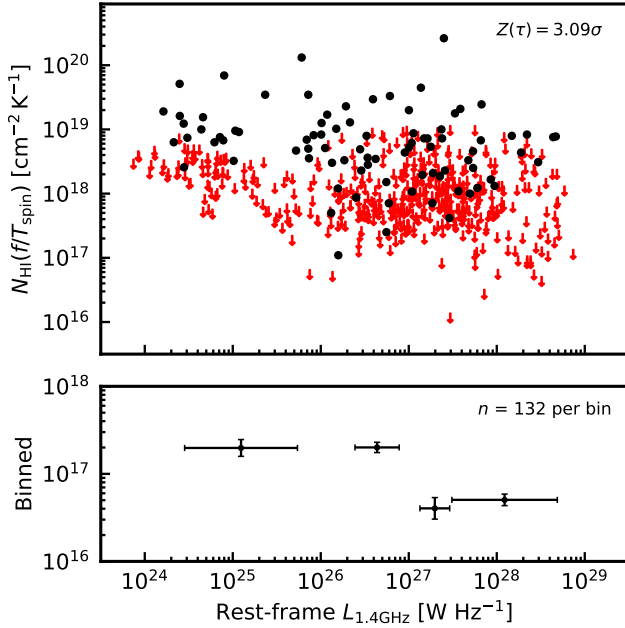


Figure 7. As Fig. 6, but for the 21-cm continuum luminosity.

Bear in mind that there will be significant noise in these data, due to different source sizes and morphologies (see Sect. 3.1.4), and the fact that a large fraction of the non-detections will simply not be orientated favourably for us to detect absorption. This would give, at best, a $\approx 50\%$ detection rate (Sect. 3.1.1) and if these could be removed, leaving only the ionisation as the factor under consideration, we could see much more significant results.

3.1.3 Radio luminosity

As stated above, Aditya & Kanekar (2018a,b) propose the excitation of the hydrogen by 1.4 GHz photons as a factor in the decrease in detection rate with redshift, although this was ruled out by Curran et al. (2008b). Returning to this, in Fig. 7 we see that the HI absorption strength also exhibits an anti-correlation with the 21-cm continuum luminosity, although with $p(\tau) = 0.0020$ this is considerably weaker than for the ionising photon rate. Furthermore, unlike for Q_{HI} , it is seen that the detections and non-detections occupy a very similar range of luminosities. Quantifying this, below the maximum detected value of $L_{1.4\text{GHz}} = 4.7 \times 10^{28} \text{ W Hz}^{-1}$ there are 85 detections and 437 non-detections, giving a detection rate of 16.3%. Above the maximum detected value, the 6 non-detections therefore give a binomial probability of 0.344 (0.95σ) of the distribution arising by chance. Thus, unlike the UV luminosity, there is no evidence of a critical radio luminosity, above which HI is not detected (as previously found by Curran et al. 2008b, 2019). We also note that a correlation between the line strength and radio luminosity would be expected just from scaling with the ionising photon rate (see Fig. 5).

3.1.4 Other effects

Aditya & Kanekar (2018a,b); Aditya et al. (2024) also propose other redshift evolutionary effects as the cause of the decrease in detection rate with redshift. Regarding each of these:

- *Source morphology*: It has long been known that the HI absorption strength is anti-correlated with the size of the source (Pihlström et al., 2003), which Curran et al. (2013c) suggested is a geometry effect introduced by the covering factor, and so we do expect higher detection rates in compact objects. However, given that HI is detected over a range of source sizes, and neither compact nor non-compact objects are detected above the critical UV luminosity (Curran & Whiting, 2010), the ionisation argument remains the more comprehensive.
- *Gas properties*: Evolving gas properties could arise from either a changing column density or evolving spin temperature (see Sects. 3.2 & 3.3). Due to the weakness of HI 21-cm emission, we do not usually have a measure of N_{HI} at $z \gtrsim 0.1$, although, from the spectra of damped Lyman- α absorption systems (DLAs), there is no evidence of any evolution for intervening absorbers (Curran 2019 and references therein). Another possibility is an increase in the spin temperature of the gas (cf. the decrease in covering factor above). However, this would be expected to be a result of the high ionisation rates.
- *AGN luminosity*: Again, this would be a signature of the ionising photon rate, since we have ruled out the effect of the radio luminosity (Sect. 3.1.3).

Aditya & Kanekar also propose an unspecified evolutionary effect. Due to the Malmquist bias, the ionising photon rate is strongly correlated with the redshift (Fig. 3) and we can test this as above: The maximum redshift at which HI has been detected is $z = 3.530$ (Aditya et al., 2021). Below this redshift, there are 90 detections and 711 non-detections with $N_{\text{HI}} \leq 10^{19} (T_{\text{spin}}/f) \text{ cm}^{-2}$, giving a detection rate of 11.2%. Thus, the binomial probability of obtaining 0 detections out of 12 at $z > 3.530$ is $p = 0.240$ (1.17σ). That is, the detection of HI appears to be much more dependent on the photo-ionisation than the redshift, although both properties are intimately entwined.

3.2 High column density systems

In Galactic high latitude clouds, above column densities of $N_{\text{HI}} \approx 4 \times 10^{20} \text{ cm}^{-2}$ (Reach et al., 1994; Heithausen et al., 2001)⁷ the HI begins to form H_2 , with Schaye (2001) suggesting that this is the reason why high redshift absorbers (DLAs) are never found with column densities $N_{\text{HI}} \gtrsim 10^{22} \text{ cm}^{-2}$. Applying this to the current sample, Curran & Whiting (2012) used a simple exponential model of the Galactic gas distribution, $n = n(0)e^{-r/R}$, where R is the scale-length of

⁷This limit is also apparent in the near-by Circinus galaxy (Curran et al., 2008a).

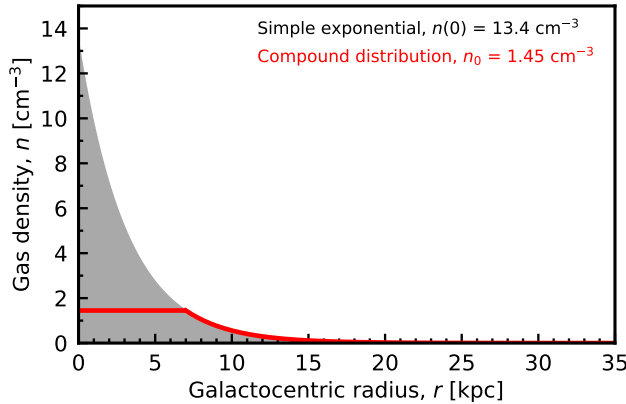


Figure 8. The gas density versus the galactocentric radius for the simple exponential (grey) and compound (red) models of the Milky Way. r_0 is radius at which the break between the models occurs.

the decay. Extrapolating from $n = n_0 e^{-(r-R_\odot)/R}$, where $n_0 = 0.9 \text{ cm}^{-3}$, $R_\odot = 8.5 \text{ kpc}$ and $R = 3.15 \text{ kpc}$ (Kalberla & Kerp, 2009) to $r = 0$, gave $n(0) = 13.4 \text{ cm}^{-3}$. The total column density between the continuum source and ourselves is therefore

$$N_{\text{HI}} = \int_0^\infty n dr = n(0) \int_0^\infty e^{-r/R} dr = n(0)R$$

$= 1.3 \times 10^{23} \text{ cm}^{-2}$, which is about an order of magnitude higher than that expected.

We therefore proceed by using a compound model, where a constant density component is added over $0 \leq r \leq r_0$ to the exponential component (Fig. 8), giving

$$N_{\text{HI}} = \int_0^{r_0} n_0 dr + \int_{r_0}^\infty n_0 e^{-(r-R_\odot)/R} dr, \quad (8)$$

where $n_0 = 0.9 \text{ cm}^{-3}$, $R = 3.15 \text{ kpc}$, $R_\odot = 8.5 \text{ kpc}$ and $r_0 = 7 \text{ kpc}$ (Kalberla & Kerp, 2009). To reduce the number of free parameters, we rewrite the formula of Kalberla & Kerp

$$n = n_0 e^{-(r-R_\odot)/R} \text{ as } n = n_0 e^{-(r-r_0)/R},$$

where $n = 0$ is now the gas density at r_0 , e.g. $n_0 = 1.45 \text{ cm}^{-3}$ at $r_0 = 7 \text{ kpc}$, cf. $n_0 = 0.9 \text{ cm}^{-3}$ at $R_\odot = 8.5 \text{ kpc}$ for the Milky Way (Fig. 8). Making the substitution and integrating, Equ. 8 becomes

$$N_{\text{HI}} = n_0 \left(r_0 + R e^{-r_0/R} \right), \quad (9)$$

giving $N_{\text{HI}} = 3.3 \times 10^{22} \text{ cm}^{-2}$, which is closer to the expected limit.

Since this value is obtained through an inclined disk, we may expect it to be close to representing the theoretical limit. For the five HI absorbers with $N_{\text{HI}} \gtrsim 10^{20} (T_{\text{spin}}/f) \text{ cm}^{-2}$ the absorption is optically thick and so the approximation in Equ. 6 cannot be used unless $f = 1$. In any case, having

Table 1 The five $N_{\text{HI}} \gtrsim 10^{20} (T_{\text{spin}}/f) \text{ cm}^{-2}$ absorbers (Chowdhury et al., 2020; Murthy et al., 2021; Su et al., 2022; Aditya et al., 2024). $N_{\text{HI}}/(f/T_{\text{spin}})$ gives the normalised absorption strength, followed by the spin temperature for $N_{\text{HI}} = 3.3 \times 10^{22} \text{ cm}^{-2}$.

Source	z	$N_{\text{HI}}/(f/T_{\text{spin}})$	T_{spin}
WISEA J022928.93+004429.5	1.217	1.35×10^{20}	$\gtrsim 240$
RCS 01020400291	1.163	1.45×10^{20}	$\gtrsim 230$
MRC 0531–237	0.851	2.63×10^{20}	$\gtrsim 130$
SDSS J090331.57+010847.5	0.522	2.14×10^{20}	$\gtrsim 150$
WISEA J145239.38+062738.2	0.267	1.32×10^{20}	$\gtrsim 250$

$f < 1$ would have the effect of decreasing the already low spin temperatures (Table 1).

Such spin temperatures are typical of the Milky Way ($T_{\text{spin}} \lesssim 300 \text{ K}$, Strasser & Taylor 2004; Dickey et al. 2009), but may be atypical in sources host to a powerful AGN. As mentioned in Sect. 3.1.1, the ionising photon rate is only available for one of these (WISEA J145239.38+062738.2), which has $Q_{\text{HI}} = 2.4 \times 10^{53} \text{ s}^{-1}$. This is three orders of magnitude below the highest value where HI has been detected. Furthermore, this, and the other three high column density systems, are at redshifts $z \ll 3$, meaning that the optical-band observation which yielded the redshift are not close to the rest-frame UV band. This was identified as introducing a possible bias by Curran et al. (2008b), where the selection of objects faint in the B -band at $z \gtrsim 3$, which were sufficiently bright to yield an optical redshift, selected only objects which were very UV luminous in the source rest-frame.

Of the three high redshift exceptions where HI has been detected, two⁸ have relatively low photo-ionisation rates ($Q_{\text{HI}} \lesssim 10^{54} \text{ s}^{-1}$, see Fig.3). For these, the redshifts were obtained from spectroscopy of the near-infrared band (Lawrence et al. 1995; Lilly et al. 1985, respectively), thus remaining clear of the rest-frame $\lambda \leq 1216 \text{ \AA}$ range, where the hydrogen becomes excited and subsequently ionised. For the other $z \gtrsim 3$ detection (8C 0604+728 at $z = 3.530$, Aditya et al. 2021), the redshift was obtained by deep optical observations towards a previously identified radio source (Jorgenson et al., 2006).⁹

3.3 HI 21-cm absorption at the highest ionisation rate

From our fitting, the highest ionising photon rate at which HI absorption has been detected (Aditya & Kanekar, 2018a) occurs at $Q_{\text{HI}} = 2.9 \times 10^{56} \text{ s}^{-1}$, in PKS 1200+045 at $z = 1.226$ (Fig. 6). This is the same as the theoretical Q_{HI} required to ionise all of the gas in the Milky Way (Curran & Whiting, 2012). However, this was based on the simple exponential distribution, which we have shown to overestimate the column

⁸J0414+0534 at $z = 2.636$, (Moore et al., 1999) and 0902+34 at $z = 3.398$ (Uson et al., 1991).

⁹Aditya et al. (2021) claim $Q_{\text{HI}} \approx 2 - 5 \times 10^{56} \text{ s}^{-1}$ for this source, although our photometry search could only find a single value with $\log_{10} \nu \geq 15.1$. in the rest-frame. Nevertheless, this ionising photon rate remains in the ballpark of the critical value.

density (Sect. 3.2).

To obtain a revised value of the critical ionising photon rate, we again start with the ionisation and recombination of the gas in equilibrium (Osterbrock, 1989),

$$Q_{\text{HI}} = 4\pi \int_0^{r_{\text{str}}} n_{\text{p}} n_{\text{e}} \alpha_A r^2 dr \quad (10)$$

where n_{p} and n_{e} are the proton and electron densities, respectively, and α_A the radiative recombination rate coefficient of hydrogen. We use here the canonical $T = 10\,000$ K for ionised gas, giving $\alpha_A = 4.19 \times 10^{-13} \text{ cm}^3 \text{ s}^{-1}$ (Osterbrock & Ferland, 2006).¹⁰ For a neutral plasma, $n_{\text{p}} = n_{\text{e}} = n$, and for complete ionisation of the gas ($r_{\text{str}} = \infty$), the compound model gives

$$Q_{\text{HI}} = 4\pi\alpha_A n_0^2 \left(\left[\frac{r^3}{3} \right]_0^{r_0} + \int_{r_0}^{\infty} e^{-2(r-r_0)/R} r^2 dr \right) \quad (11)$$

$$= \pi\alpha_A n_0^2 \left(\frac{4r_0^3}{3} + R [2r_0^2 + 2Rr_0 + R^2] \right), \quad (12)$$

which for $r_0 = 0$ becomes the simple exponential model at large radii, $Q_{\text{HI}} = \pi\alpha_A n_0^2 R^3$ (Curran & Whiting, 2012). An important feature of this is that the radius of the Ström-gren sphere becomes infinite for a finite photo-ionisation rate, giving the abrupt cut-off in HI detections seen in the observations.

From Equ. 12, the ionising photon rate to ionise all of the gas in the Milky Way is revised to $Q_{\text{HI}} = 7.6 \times 10^{55} \text{ s}^{-1}$, which is a factor of four lower than for the simple exponential model. Of course all of gas need not be ionised to be rendered below the detection limits of current radio telescopes, although the apparently abrupt cut-off in the detection of HI at $Q_{\text{HI}} \gtrsim 10^{56} \text{ s}^{-1}$ has persisted in all of the published searches since Curran et al. (2008b) [see Sect. 1].

In Fig. 9 we show the “tweaking” required to the Galactic gas distribution to increase the critical value to $Q_{\text{HI}} = 2.9 \times 10^{56} \text{ s}^{-1}$. For example, for the same values of R and r_0 as the Milky Way, the central density would have to be doubled to $n_0 = 2.9 \text{ cm}^{-3}$. Conversely, keeping $n_0 = 1.45 \text{ cm}^{-3}$ gives the values of r_0 and R listed in Table 2. From these parameters we estimate column densities which are approximately equal to the maximum expected (Sect. 3.2) and use these to estimate possible T_{spin}/f values, all of which are very high. While low covering factors ($f \ll 1$) could contribute to these, high spin temperatures would be expected from the strong UV continuum (Field, 1959; Bahcall & Ekers, 1969).¹¹

In the table we also show the total gas masses, obtained from $M_{\text{gas}} = \int_0^{\infty} \rho dV$, where the volume of the disk gives $dV = 2\pi t r dr$, with t being its thickness. In the Galaxy the thickness is related to the galactocentric radius via the flare

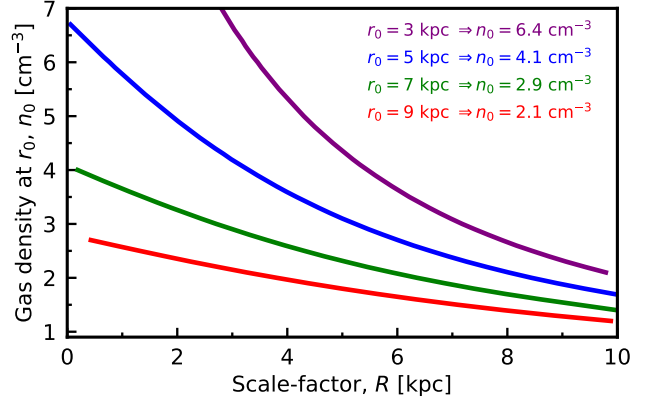


Figure 9. The gas density at r_0 versus the scale-length required for all of the gas to be ionised by $Q_{\text{HI}} = 2.9 \times 10^{56} \text{ s}^{-1}$. $r_0 = 7$ kpc for the Milky Way (Kalberla & Kerp, 2009) and the key shows the value of n_0 required for the Milky Way’s $R = 3.15$ kpc.

Table 2 The required scale-length for various values of r_0 to yield complete ionisation for $Q_{\text{HI}} = 2.9 \times 10^{56} \text{ s}^{-1}$ and $n_0 = 1.45 \text{ cm}^{-3}$. The column densities are calculated from Equ. 9 and T_{spin}/f from the measured $N_{\text{HI}} = 4.6 \times 10^{18} (T_{\text{spin}}/f) \text{ cm}^{-2}$ (Aditya & Kanekar, 2018a). The gas masses are calculated from Equ. 14 using the Galactic flare factor (Kalberla & Kerp, 2009).

r_0 [kpc]	R [kpc]	$N_{\text{HI}} [\text{cm}^{-2}]$	T_{spin}/f [K]	$M_{\text{gas}} [M_{\odot}]$
< 7	> 10	$\lesssim 4 \times 10^{22}$	$\lesssim 9000$	$\gtrsim 4 \times 10^{10}$
7.0	9.3	5.3×10^{22}	12 000	3.5×10^{10}
8.0	8.2	5.1×10^{22}	11 000	3.3×10^{10}
9.0	7.1	5.1×10^{22}	11 000	3.1×10^{10}
10.0	5.9	5.1×10^{22}	11 000	2.8×10^{10}
11.0	4.5	5.3×10^{22}	12 000	2.4×10^{10}
12.0	3.0	5.6×10^{22}	12 000	1.9×10^{10}
$\gtrsim 13$	$\lesssim 1$	$\gtrsim 6 \times 10^{22}$	$\gtrsim 13\,000$	$\lesssim 1 \times 10^{10}$

¹⁰<http://amdpp.phys.strath.ac.uk/tamoc/DATA/RR/>

¹¹With an absorption strength of $N_{\text{HI}} = 7.8 \times 10^{18} (T_{\text{spin}}/f) \text{ cm}^{-2}$, this model yields $T_{\text{spin}}/f \approx 6000$ K for 8C 0604+728 at $z = 3.530$ (see previous section).

factor, $F = r/t \approx 20$ (Kalberla & Kerp, 2009), giving for the compound model

$$M_{\text{gas}} = \frac{2\pi}{F} n_0 m_p \left(\left[\frac{r^3}{3} \right]_0^{r_0} + \int_{r_0}^{\infty} e^{-(r-r_0)/R} r^2 dr \right), \quad (13)$$

which gives

$$M_{\text{gas}} = \frac{2\pi}{F} n_0 m_p \left(\frac{r_0^3}{3} + R [r_0^2 + 2Rr_0 + 2R^2] \right). \quad (14)$$

The HI masses derived from Equ. 14 (Table 2) are close to the maximum observed in 1000 low redshift galaxies ($M_{\text{gas}} = 4 \times 10^{10} M_{\odot}$, Koribalski et al. 2004), indicating that $Q_{\text{HI}} \sim 3 \times 10^{56} \text{ s}^{-1}$ is approaching the critical value above which all of the gas in most galaxies will be ionised.

4 CONCLUSIONS

From the complete photometry of each of the 924 $z \geq 0.1$ radio sources searched for in HI 21-cm absorption, we have collated the ionising photon rates and radio luminosities, finding:

- The highest ionising photon rate at which HI has been detected remains $Q_{\text{HI}} \approx 3 \times 10^{56} \text{ s}^{-1}$, which is close to the value required to ionise all of the neutral gas in a large spiral galaxy, thus confirming that the dearth of HI detections at high redshift is due to the bias towards sources which are most UV luminous in the rest-frame.
- Both the ionising photon rate and radio luminosity are anti-correlated with the strength of the HI absorption, although the Q_{HI} correlation is the strongest. Also, unlike the ionising photon rate, there is no critical radio luminosity above which HI is not detected. That is, ionisation of the gas, rather than excitation to the upper hyper-fine level, appears to be the dominant mechanism for the dearth of HI absorption at high redshift.
- Any evolution in the source morphologies or gas properties cannot explain the decrease in detection rate with redshift as holistically as the ionisation hypothesis.
- Detection rates are higher in galaxies than in quasars, which we attribute to the quasars generally being more luminous in the ultra-violet. It is possible that orientation effects play a role, although being a type-1 object does not necessarily exclude the detection of HI absorption. This suggests that the absorption primarily occurs in the large-scale galactic disk, as opposed to the pc-scale obscuring torus.

From the total neutral hydrogen column density of the Milky Way (Kalberla & Kerp, 2009), and that expected from theory, we find:

- The strengths of the five recently detected HI absorbers with $N_{\text{HI}} \gtrsim 10^{20} (T_{\text{spin}}/f) \text{ cm}^{-2}$ (Chowdhury et al., 2020; Murthy et al., 2021; Su et al., 2022; Aditya et al., 2024), imply spin temperatures of $T_{\text{spin}}/f \lesssim 300 \text{ K}$,

which are typical of the Milky Way (Strasser & Taylor, 2004; Dickey et al., 2009). Sufficient UV photometry to obtain the ionising photon rate is only available for one of these, but with $Q_{\text{HI}} = 2.4 \times 10^{53} \text{ s}^{-1}$ this is three orders of magnitude below the critical value above which we expect all of the gas to be ionised.

- Conversely, for the detection of HI at the highest ionising photon rate ($Q_{\text{HI}} = 2.9 \times 10^{56} \text{ s}^{-1}$), we estimate $T_{\text{spin}}/f \sim 12000 \text{ K}$ which is consistent with a high ionisation fraction.
- At this ionising photon rate we calculate a gas mass of $M_{\text{gas}} \approx 3 \times 10^{10} M_{\odot}$, which is close to the maximum value observed in a survey of a 1000 low redshift galaxies (Koribalski et al., 2004).

The model is, of course, an idealisation, based upon the gas distribution of the Milky Way and taking no account of shielding by dust¹² or regions of denser gas (e.g. molecular clouds). However, it is remarkable that it comes close to yielding the maximum ionising photon rate at which HI has been detected for a gas distribution so similar to that of a large spiral galaxy. Thus, both the extensive observational results and the model suggest that ionisation by $\lambda \leq 912 \text{ \AA}$ photons is the dominant reason for the non-detection of cold, neutral gas within the host galaxies of high redshift radio sources.

DATA AVAILABILITY

Data available on request.

ACKNOWLEDGEMENTS

I would like to thank the anonymous referee for their prompt and supportive feedback. This research has made use of the NASA/IPAC Extragalactic Database (NED) which is operated by the Jet Propulsion Laboratory, California Institute of Technology, under contract with the National Aeronautics and Space Administration and NASA's Astrophysics Data System Bibliographic Service. This research has also made use of NASA's Astrophysics Data System Bibliographic Service and ASURV Rev 1.2 (Lavalley et al., 1992), which implements the methods presented in Isobe et al. (1986).

REFERENCES

- Aditya J. N. H. S., Kanekar N., 2018a, MNRAS, 473, 59
 Aditya J. N. H. S., Kanekar N., 2018b, MNRAS, 481, 1578
 Aditya J. N. H. S., Kanekar N., Kurapati S., 2016, MNRAS, 455, 4000
 Aditya J. N. H. S., Jorgenson R., Joshi V., Singh V., An T., Chandola Y., 2021, MNRAS, 500, 998
 Aditya J. N. H. S., et al., 2024, MNRAS, 527, 8511
 Allison J. R., et al., 2012, MNRAS, 423, 2601
 Antonucci R. R. J., 1993, ARA&A, 31, 473

¹²Which may be countered somewhat by the UV photometry being uncorrected for dust, rendering the values as relative rather than absolute.

- Antonucci R. R. J., Miller J. S., 1985, *ApJ*, 297, 621
- Bahcall J. N., Ekers R. D., 1969, *ApJ*, 157, 1055
- Chowdhury A., Kanekar N., Chengalur J. N., 2020, *ApJ*, 900, L30
- Curran S. J., 2012, *ApJ*, 748, L18
- Curran S. J., 2019, *MNRAS*, 484, 3911
- Curran S. J., 2020, *A&A*, 635, A166
- Curran S. J., Whiting M. T., 2010, *ApJ*, 712, 303
- Curran S. J., Whiting M. T., 2012, *ApJ*, 759, 117
- Curran S. J., Koribalski B. S., Bains I., 2008a, *MNRAS*, 389, 63
- Curran S. J., Whiting M. T., Wiklind T., Webb J. K., Murphy M. T., Purcell C. R., 2008b, *MNRAS*, 391, 765
- Curran S. J., et al., 2011, *MNRAS*, 413, 1165
- Curran S. J., Whiting M. T., Sadler E. M., Bignell C., 2013a, *MNRAS*, 428, 2053
- Curran S. J., Whiting M. T., Tanna A., Sadler E. M., Pracy M. B., Athreya R., 2013b, *MNRAS*, 429, 3402
- Curran S. J., Allison J. R., Glowacki M., Whiting M. T., Sadler E. M., 2013c, *MNRAS*, 431, 3408
- Curran S. J., Allison J. R., Whiting M. T., Sadler E. M., Combes F., Pracy M. B., Bignell C., Athreya R., 2016, *MNRAS*, 457, 3666
- Curran S. J., Whiting M. T., Allison J. R., Tanna A., Sadler E. M., Athreya R., 2017a, *MNRAS*, 467, 4514
- Curran S. J., Hunstead R. W., Johnston H. M., Whiting M. T., Sadler E. M., Allison J. R., Bignell C., 2017b, *MNRAS*, 470, 4600
- Curran S. J., Hunstead R. W., Johnston H. M., Whiting M. T., Sadler E. M., Allison J. R., Athreya R., 2019, *MNRAS*, 484, 1182
- Deka P. P., et al., 2024, *A&A*
- Dickey J. M., Strasser S., Gaensler B. M., Haverkorn M., Kavars D., McClure-Griffiths N. M., Stil J., Taylor A. R., 2009, *ApJ*, 693, 1250
- Field G. B., 1959, *ApJ*, 129, 536
- Geréb K., Maccagni F. M., Morganti R., Oosterloo T. A., 2015, *A&A*, 575, 44
- Grasha K., Darling J. K., Bolatto A. D., Leroy A., Stocke J., 2019, *ApJS*, 245, 3
- Heithausen A., Brüns C., Kerp J., Weiss A., 2001, in Pilbratt G. L., Cernicharo J., Heras A. M., Prusti T., Harris R., eds, Vol. 460, *The Promise of the Herschel Space Observatory*. p. 431
- Isobe T., Feigelson E., Nelson P., 1986, *ApJ*, 306, 490
- Jorgenson R. A., Wolfe A. M., Prochaska J. X., Lu L., Howk J. C., Cooke J., Gawiser E., Gelino D. M., 2006, *ApJ*, 646, 730
- Kalberla P. M. W., Kerp J., 2009, *Ann. Rev. Astr. Ap.*, 47, 27
- Kaplan E. L., Meier P., 1958, *J. Amer. Statist. Assoc.*, 53, 457
- Koribalski B. S., et al., 2004, *AJ*, 128, 16
- Lavalley M. P., Isobe T., Feigelson E. D., 1992, in *BAAS*. pp 839–840
- Lawrence C. R., Cohen J. G., Oke J. B., 1995, *AJ*, 110, 2583
- Lilly S. J., Longair M. S., Allington-Smith J. R., 1985, *MNRAS*, 215, 37
- Maccagni F. M., Morganti R., Oosterloo T. A., Geréb K., Maddox N., 2017, *A&A*, 604, A43
- Mahony E. K., et al., 2022, *MNRAS*, 509, 1690
- Miller J. S., Goodrich B. F., 1987, *BAAS*, 19, 695
- Moore C. B., Carilli C. L., Menten K. M., 1999, *ApJ*, 510, L87
- Morgan W. W., Whitford A. E., Code A. D., 1953, *ApJ*, 118, 318
- Murthy S., Morganti R., Oosterloo T., Maccagni F. M., 2021, *A&A*, 654, A94
- Murthy S., Morganti R., Kanekar N., Oosterloo T., 2022, *A&A*, 659, A185
- Osterbrock D. E., 1978, *Proc. Nat. Acad. Sci.*, 75, 540
- Osterbrock D. E., 1989, *Astrophysics of Gaseous Nebulae and Active Galactic Nuclei*. University Science Books, Mill Valley, California
- Osterbrock D. E., Ferland G. J., 2006, *Astrophysics of Gaseous Nebulae and Active Galactic Nuclei*. University Science Books, Sausalito, California
- Pihlström Y. M., Conway J. E., Vermeulen R. C., 2003, *A&A*, 404, 871
- Planck Collaboration et al., 2020, *A&A*, 641, A6
- Purcell E. M., Field G. B., 1956, *ApJ*, 124, 542
- Reach W. T., Koo B.-C., Heiles C., 1994, *ApJ*, 429, 672
- Schaye J., 2001, *ApJ*, 562, L95
- Skrutskie M. F., et al., 2006, *AJ*, 131, 1163
- Strasser S., Taylor A. R., 2004, *ApJ*, 603, 560
- Su R., et al., 2022, *MNRAS*, 516, 2947
- Su R., et al., 2023, *ApJ*, 956, L28
- Uson J. M., Bagri D. S., Cornwell T. J., 1991, *PhRvL*, 67, 3328
- Vermeulen R. C., et al., 2003, *A&A*, 404, 861
- Wright E. L., et al., 2010, *AJ*, 140, 1868